AIP Publishing

This manuscript was accepted by J. Chem. Phys. Click here to see the version of record.

The Binding Energy and Dynamics of Charge-Transfer States in Organic Photovoltaics with Low Driving Force for Charge Separation

Yifan Dong,[1] Hyojung Cha,[1] Jiangbin Zhang,[1,2] Ernest Pastor,[1] Pabitra Shakya Tuladhar,[1] Iain McCulloch,[1,3] James R. Durrant,[1,4*] Artem A. Bakulin[1*]

[1]*Department of Chemistry and Centre for Plastic Electronics, Imperial College London, London SW7 2AZ, United Kingdom*

[2]*Cavendish Laboratory, University of Cambridge, JJ Thomson Avenue, Cambridge CB3 0HE, United Kingdom*

[3]*Physical Sciences and Engineering Division, KAUST Solar Centre (KSC), King Abdullah University of Science and Technology (KAUST), KSC Thuwal 23955-6900, Saudi Arabia*

[4]*SPECIFIC IKC, College of Engineering, Swansea University, Swansea SA12 7AX, United Kingdom*

ACCEPTED MANUSCRIPT

Abstract

Recent progress in organic photovoltaics (OPVs) has been enabled by optimization of the energetic driving force for charge separation, and thus maximization of open-circuit voltage, using non-fullerene acceptor (NFA) materials. In spite of this, the carrier dynamics and relative energies of the key states controlling the photophysics of these systems are still under debate. Herein, we report an in-depth ultrafast spectroscopic study of a representative OPV system based on a polymer donor PffBT4T-2OD and a small-molecule NFA EH-IDTBR. Global analysis of the transient absorption data reveals efficient energy transfer between donor and acceptor molecules. The extracted kinetics suggest that slow (~15 ps) generation of charge carriers is followed by significant geminate recombination. This contrasts with the 'reference' PffBT4T-2OD:$PC_{71}BM$ system where bimolecular recombination dominates. Using temperature-dependent pump-push-photocurrent spectroscopy, we estimate the activation energy for the dissociation of bound charge-transfer states in PffBT4T-2OD:EH-IDTBR to be 100 ± 6 meV. We also observe an additional activation energy of 14 ± 7 meV, which we assign to the de-trapping of mobile carriers. This work provides a comprehensive picture of photophysics in a system representing new generation of OPV blends with small driving force for charge separation.

AIP Publishing

This manuscript was accepted by J. Chem. Phys. Click here to see the version of record.

1. Introduction

Most organic photovoltaic (OPV) devices employ the bulk-heterojunction architecture with an interpenetrating network of electron donor (D) and electron acceptor (A) organic molecules as the absorber materials.[1] While the role of D materials has been traditionally played by a wide variety of conjugated polymers, the role of acceptors was usually taken by fullerene and its derivatives, like [6,6]-phenyl-C71-butyric acid methyl ester ($PC_{71}BM$). However, over the past few years, a new class of small molecules known as non-fullerene acceptors (NFAs) have been developed to replace fullerenes.[2–7] When mixed with common polymer donors including P3HT, PTB7-Th and PffBT4T-2OD, NFA-based blends show enhanced open-circuit voltage (V_{OC}) and increased stability compared to their fullerene counterparts.[8–15] The most efficient single-junction OPV to date has reached a power conversion efficiency of 14% using the NFA ITIC-4F.[16] Despite this rapid rise in efficiency, a fundamental understanding of the charge generation mechanism is still lagging behind.

Bound electron-hole pairs, excitons, are generated in D and A materials upon photoexcitation. Excitons dissociate at the D/A interface and form interfacial charge-transfer states (CTSs). This process can be driven by the energetic difference between the lowest unoccupied molecular orbitals (LUMOs) or the highest occupied molecular orbitals (HOMOs) of D and A. It has been widely reported that free charges can be generated from these intermediate CTSs, leading to photocurrent generation in devices. However the detailed mechanism of charge separation from CTSs remains controversial.[17–20] The energy of the CTS, E_{CT}, is related to the energetic difference between the HOMO of D and the LUMO of A, which limits the attainable V_{OC}.[21] The remarkably high V_{OC} in NFA-based blends has been achieved by increasing E_{CT} via matching the LUMO or HOMO level of the acceptor closer to that of D.[22–24] This implies that a smaller driving force for charge separation is a common feature among the state-of-the-art NFA-based OPVs.[25,26] Understanding how the smaller driving force affects the dynamics of CTSs is hence crucial to improve the charge generation in NFA-based OPVs.

One of the NFA-based benchmark systems with a low driving force for charge separation is PffBT4T-2OD:EH-IDTBR. PffBT4T-2OD is a polymer donor which was first reported by Yan and coworkers.[27] It exhibits strong aggregation ability and tends to form highly crystalline domains.[27] The NFA EH-IDTBR was reported by the McCulloch group in 2016.[10] It is based on

ACCEPTED MANUSCRIPT

AIP Publishing

This manuscript was accepted by J. Chem. Phys. Click here to see the version of record.

indacenodithiophene core with ethyl hexyl side chains. The planar conjugation together with the highly electron-rich core raises the LUMO, thereby increasing E_{CT} relative to fullerene-based blends. EH-IDTBR also exhibits a high molar extinction coefficient (~10^5 M^{-1} cm^{-1}) in solutions and a higher absorption coefficient in thin films than some polymer donors.[10] This opens up the possibility for hole transfer to be as equally important as electron transfer for charge generation in devices.

In our previous work on PffBT4T-2OD:EH-IDTBR and PffBT4T-2OD:$PC_{71}BM$, we reported relatively long exciton quenching times (30 ± 2 ps) in both systems, that are still much shorter than the exciton lifetime in the neat PffBT4T-2OD (300 ps).[9] This agrees with the photoluminescence (PL) quenching yield (77% and 80% for EH-IDTBR and $PC_{71}BM$ systems respectively). Though similar exciton quenching kinetics and yields were observed, the yield of free carriers in the former system is lower, leading to a drop in short-circuit current (J_{SC}). Cha *et al.* attributed this to the smaller driving force for charge separation and greater degree of geminate recombination in PffBT4T-2OD:EH-IDTBR.[9,28] However, in-depth analysis of the transient absorption (TA) data have not been performed. The exciton and charge dynamics as well as the dynamics of CTS have not been clearly identified.[29] The enhanced stability and V_{OC} together with the congruent absorption between PffBT4T-2OD and EH-IDTBR make their blend an interesting system for in-depth spectroscopic studies. Previous studies have indicated the promising potential of OPV blends with overlapping absorption features. For example, Baran *et al.* have reported that blending PTB7-Th with EH-IDTBR leads to stable and efficient OPV with minimal recombination losses.[8] Also Kirchartz *et al*. have recently pointed out overlapping absorption is preferable and beneficial for OPV performance if the active layer thickness is relatively thin, which is commonly observed among NFA-based OPVs.[30]

This study goes beyond the previous work and focuses on investigating the carrier dynamics in PffBT4T-2OD:EH-IDTBR with different types of ultrafast spectroscopy tools and advanced global analysis of the TA data. The use of global analysis identifies the spectral footprints for PffBT4T-2OD excitons, EH-IDTBR excitons and charges. It reveals the ultrafast energy transfer between PffBT4T-2OD and EH-IDTBR excitons under photoexcitation. However, the subsequent exciton dissociation into CTSs appears to be slow (~15 ps). Rather than separating into free charges, a large number of CTSs remain bound and undergo geminate recombination. This differs

ACCEPTED MANUSCRIPT

AIP Publishing

This manuscript was accepted by J. Chem. Phys. Click here to see the version of record.

from the 'reference' PffBT4T-2OD:$PC_{71}BM$ system where charge separation is also efficient but is followed by bimolecular recombination. To understand the nature of CTSs in PffBT4T-2OD:EH-IDTBR, we investigate how the temperature affects charge generation using pump-push-photocurrent (PPPC) spectroscopy. PPPC measurements were employed to address the dynamics of interfacial bound states in OPVs. The early-time (< 100 ps) PPPC kinetics resemble the CTS dynamics extracted from the TA data. This implies that the same photophysical process governs the formation of CTSs. We further used the Arrhenius relation to fit the early-time PPPC traces across different temperatures to determine the activation energy (E_a) for CTS formation to be on the order of 100 ± 6 meV, which is the first reported E_a value for NFA blends. In addition, by fitting the long-time PPPC kinetics, the activation energy of charge de-trapping was determined to be 14 ± 7 meV.

II. Materials

Figure 1. (a) Normalized steady-state absorption spectra of the materials under study. (b) Normalized steady-state PL spectra for PffBT4T-2OD, EH-IDTBR and PffBT4T-2OD:EH-IDTBR blend. All samples were excited at 600 nm.

Figure 1a displays the absorption spectra of PffBT4T-2OD, EH-IDTBR, $PC_{71}BM$ and their blends. PffBT4T-2OD shows a pronounced absorbance peak at 700 nm, which has been previously assigned to the strong aggregation in the film.[27] EH-IDTBR exhibits an absorbance peak at a similar wavelength (675 nm). The absorption spectra of these two neat materials largely overlap between 500 to 800 nm. Figure 1b shows the normalized steady-state PL spectra for PffBT4T-2OD, EH-IDTBR and their blend. PffBT4T-2OD and EH-IDTBR emit at 732 and 736 nm respectively, in agreement with their previously reported bandgap values (1.69 eV and 1.68 eV). After mixing PffBT4T-2OD with EH-IDTBR, the PL emission maximum peak is broadened and shows a 'flat' peak between 732 and 736 nm. This indicates the blend emission comes from the excitons in both materials. The blend PL resembles both neat materials in the 650 to 736 nm region, while the lower energy tail (736 to 850 nm) is expanded and is probably due to the increase in disorder upon mixing. Figure S3 compares the steady-state PL with the time-resolved PL taken from time-correlated single photon counting (TCSPC) for neat PffBT4T-2OD, neat EH-IDTBR and their blend. For each material and their blend, both the steady-state and the time-resolved PL spectra resemble each other. Additionally, the emission maxima stay unchanged at different time delays (0-100 ns) for all the samples. While the emission in the neat materials is dominated by

ACCEPTED MANUSCRIPT

AIP Publishing

This manuscript was accepted by J. Chem. Phys. Click here to see the version of record.

excitons, the emission in the blend could be from both excitons and CTSs. The same PL emission peak in the blend hence suggests two possibilities: (1) the excitons and CTS emit at the same energy or (2) the radiative emission from CTSs is relatively weak to be observed. Previous studies has indicated that PffBT4T-2OD:EH-IDTBR system has small LUMO and HOMO energy differences of 0.21 and 0.24 eV respectively between D and A,[9] leading to a lower CTS energy than the excitons. However, the broadening of the lower energy tail (750 nm to 850 nm) may represent the contribution from the CTSs. The fact that D and A have low exciton energy difference (0.01 eV) makes it challenging to distinguish which material dominates the charge generation in the blend. Also, a significant number of excitons have been quenched by 100 ps which is below the time resolution of the TCSPC instrument. Therefore, we now turn to the TA data to investigate exciton separation and charge recombination kinetics over the ps to ns timescale.

III. Results and Discussion

1. Transient absorption spectroscopy

Figure 2. (a) Normalized TA spectra for the PffBT4T-2OD:$PC_{71}BM$ blend film at different pump-probe delay times. The orange dashed line indicates the same PIA peak at 1100 nm throughout the measurement. (b) Normalized TA spectra for the PffBT4T-2OD:EH-IDTBR blend film at different pump-probe delay times. The orange and green dashed lines represent the initial PIA peak at 1125 nm and the evolved PIA peak at 1080 nm. Pump wavelength was 700 nm and the fluence was 10 μJ cm^{-2} for both samples.

Figure 2 compares the time-resolved near-infrared (900 to 1400 nm) TA spectra of the two OPV blends. For the PffBT4T-2OD:$PC_{71}BM$ blend film in Figure 2a, the initial PIA peak at 1100 nm is assigned to the PffBT4T-2OD exciton. This is confirmed by comparison with the neat PffBT4T-2OD TA data (Figure S4). In neat PffBT4T-2OD, the exciton PIA peak stays at 1100 nm with minimal spectral shift over time, indicating that only PffBT4T-2OD excitons are present. In the PffBT4T-2OD:$PC_{71}BM$ blend shown in Figure 2a, the PIA peak remains at 1100 nm, but the lower energy shoulder (1100 to 1400 nm) becomes narrower within the first 100 ps. This distortion in the blend spectra indicates the appearance of another species while the PffBT4T-2OD exciton decays. Because only PffBT4T-2OD was excited, charges formed through photo-induced electron

ACCEPTED MANUSCRIPT

AIP Publishing

This manuscript was accepted by J. Chem. Phys. Click here to see the version of record.

transfer from PffBT4T-2OD to $PC_{71}BM$ are the most likely species. After 100 ps, there is no further change in the spectra. Therefore, we attribute the PIA after 100 ps solely to the charges since all the excitons have decayed.

Figure 2b shows the TA data for the PffBT4T-2OD:EH-IDTBR blend film. The initial PIA peak stays at 1125 nm, whereas the PIA peaks for neat PffBT4T-2OD and neat EH-IDTBR are at 1100 nm and 1150 nm respectively. Additionally, the spectra shape at 1 ps differs from either one of the neat materials spectra (Figure S6). Therefore, we assign the PIA peak at 1125 nm in the blend to the combination of exciton absorption from both materials due to the co-excitation under the laser pump. This PIA peak gradually shifts to 1080 nm over 50 ps. This is due to the photoinduced electron and hole transfer between PffBT4T-2OD and EH-IDTBR excitons. The co-existence of D and A excitons in NFA OPV blends have also been reported elsewhere and is becoming a common feature among NFA-based OPV systems.[25,31] For example, Laquai and coworkers observed the co-existence of cations and anions in TA formed through electron and hole transfer in PTB7-Th:CDTBM.[32] However, few studies indicate the individual dynamics of D and A exciton decay. To further understand the charge carrier dynamics of each species, we use global analysis to deconvolute the kinetics of individual excited state species from the TA data.

2. Global analysis of TA

Figure 3a and 3b show the deconvoluted spectra and the corresponding kinetics for the PffBT4T-2OD:$PC_{71}BM$ blend film using global analysis. The results clearly indicate the presence of two excited state species when PffBT4T-2OD was selectively excited by pumping at 700 nm. By comparing the spectra with the neat PffBT4T-2OD spectra (Figure S4), we assign the broad spectra feature centred at 1100 nm to PffBT4T-2OD excitons. The kinetics in Figure 3b show one component with a fast decay rate and another component being gradually formed which exhibits a longer lifetime. The fast-decaying component is PffBT4T-2OD excitons and the faster decay kinetics relative to that in neat PffBT4T-2OD TA represents the quenching due to the electron transfer to $PC_{71}BM$. The other component is hence assigned to the charges that are generated as a result of charge transfer. Fitting the kinetics in Figure 3b yields a quenching time of 15 ps for PffBT4T-2OD excitons. A notable feature here is the slow formation of charges which was also observed before in TA for the same blend.[33] This is in contrast with other well intermixed

ACCEPTED MANUSCRIPT

AIP Publishing

This manuscript was accepted by J. Chem. Phys. Click here to see the version of record.

fullerene-based OPV systems where charge generation is much faster (~ 200 fs).[34–36] The slow generation here may be associated with the relatively large domain size of PffBT4T-2OD aggregates in PffBT4T-2OD:$PC_{71}BM$ blend as shown in the TEM (Figure S7).[29]

Figure 3 Deconvoluted spectra (a, c) and kinetics (b, d) for PffBT4T-2OD: $PC_{71}BM$ and PffBT4T-2OD: EH-IDTBR blends. Samples were excited at 715 nm with a fluence of 10 μJ/cm^2.

Similarly, Figure 3c and 3d show the deconvoluted spectra and the corresponding kinetics for each species in the PffBT4T-2OD:EH-IDTBR blend. The deconvoluted spectra in Figure 3c indicates three distinct PIA spectra centred at 1080, 1100 and 1150 nm individually. As discussed earlier, both PffBT4T-2OD and EH-IDTBR excitons are present under illumination. Comparing with the neat material spectra (Figure S4 and S5), we therefore assign the broad PIA feature centring at 1100 nm to PffBT4T-2OD excitons and the narrower PIA at 1150 nm to EH-IDTBR excitons. As shown in the TA data (Figure 2b), the PIA peak of the long-lived charges shifts to 1080 nm. We therefore assign the third component with an absorption peak at 1080 nm to the feature of charges. Turning to the kinetics in Figure 3d, both PffBT4T-2OD and EH-IDTBR excitons decay with the same quenching time of 9 ps, comparable to previous studies.[29] The same decay time of both excitons provides evidence that PffBT4T-2OD exciton and EH-IDTBR exciton are going through ultrafast energy transfer due to their similar exciton energies (1.68 and 1.69 eV). While the excitons decay, charges are generated with a similar time constant of 10-15 ps and subsequently decay with a time constant of 1.2 ns. Though the TEM shows an intermixed morphology in the PffBT4T-2OD:EH-IDTBR blend (see TEM in Figure S7), the quenching time of excitons and the generation time of charges still happen on a shorter timescale compared to other finely mixed fullerene blends, in which the excitons typically dissociate on an ultrafast (~200 fs) timescale.[37–39]

We note that the yield of charges at 6 ns is relatively low in the PffBT4T-2OD:EH-IDTBR blend (only 25% of charges escape the recombination pathway and contribute to the long-lived charge generation). One possible reason is the acceleration of the exciton and charge dynamics due to the exciton-exciton or exciton-charge annihilation at slightly high pump fluences. To exclude this contribution and to distinguish which recombination pathway dominates for each blend, we also performed the same TA measurements and global analysis under various pump fluences.

ACCEPTED MANUSCRIPT

AIP Publishing

This manuscript was accepted by J. Chem. Phys. Click here to see the version of record.

Figure 4 Deconvoluted kinetics of charges for (a) PffBT4T-2OD:$PC_{71}BM$ blend and (b) PffBT4T-2OD:EH-IDTBR at different pump fluences from global analysis. Solid lines are multiexponential fittings as guide to the eyes.

Figure 4a displays the charge dynamics at various pump fluences extracted from global analysis for PffBT4T-2OD:$PC_{71}BM$. As the pump fluence decreases, the amplitude representing the yield of charges drops proportionally. While the generation kinetics are mostly independent on the pump fluence, the recombination kinetics are strongly fluence-dependent. At a lower pump fluence, we observe a much slower decay with more charges remaining across our measurement timescale. The charge lifetime gradually increases from 0.8 to 15 ns as the fluence decreases from 20 to 2.5 $\mu J/cm^2$. From the fluence-dependent dynamics, it indicates negligible geminate losses and the main loss is the bimolecular recombination of charges as observed by Cha et al.[9] Figure 4b displays the charge kinetics for PffBT4T-2OD:EH-IDTBR extracted from global analysis for TA carried out at various fluences. Compared to the $PC_{71}BM$ blend, here the charge generation time is slower (~15 ps) at the lowest fluence of 2.5 $\mu J/cm^2$). The recombination kinetics show fluence-independent behaviour, which indicates that the geminate recombination pathway dominates. A significant amount of charges are already recombined by 5 ns even at a lower fluence similar to 1 Sun condition (2.5 $\mu J/cm^2$). Comparing the kinetics of charges in these two blends at the same fluence, we always observe a higher recombination loss and a faster decay kinetics in the PffBT4T-2OD:EH-IDTBR blend.

3. Pump-push-photocurrent spectroscopy

Pump-push-photocurrent (PPPC) measurements have previously been employed to probe the dynamics of bound CTSs at molecular interfaces. PPPC is hence employed here to address the dissociation dynamics of CTSs by probing the photocurrent change in PffBT4T-2OD:EH-IDTBR devices. In OPVs, charge transfer of excitons at the D/A interface generates CTSs which then go through relaxation to localized states. The successful escape of the electron and hole from CTSs generates free carriers and this dissociation efficiency is directly related to the photocurrent in devices.[40] In PPPC measurements, the yield of free carriers and the charge extraction efficiency (η_{ext}) determine the reference current (J) which is measured when the cell is illuminated by the 650 nm pump beam only. The later arrival of the IR push pulse (2000 nm) excites the localized bound CTSs into higher energy states and assists the dissociation of CTSs into free carriers with a certain

ACCEPTED MANUSCRIPT

AIP Publishing

This manuscript was accepted by J. Chem. Phys. Click here to see the version of record.

probability (P_{dis}). For technical reasons, 2000 nm push was used. However, the dynamics at both 1300 nm and 2000 nm push appeared to be similar as shown in our previous work.[33] Therefore, we assign the signal to the optical activation of localized immobile charged states that can be CTS or separated carriers in the shallow traps. As a result of this push beam, extra photocurrent (ΔJ) is generated. The additional photocurrent, ΔJ, is linked with the product of the number of localised CTSs (N_{CT}), dissociation probability (P_{dis}) and the charge extraction efficiency (η_{ext}).[41] Varying the time delays between the pump and push pulses up to 2 ns, we can monitor how the population of bound CTSs changes as a function of time.

Figure 5a presents the early time PPPC kinetics for the PffBT4T-2OD:EH-IDTBR device. We narrow our analysis down to the first 100 ps time window where the kinetics show a slow rise with a time constant of 15 ps. We attribute this signal to the formation of localized CTSs. The slow generation of CTSs has been reported recently for other OPV systems.[22,39,42] As mentioned before for the $PC_{71}BM$ case, the slow diffusion of excitons across the relatively large PffBT4T-2OD domains could be one of the reasons for this slow generation of CTSs.[29,43] Another possible reason could be the high activation barrier to form CTSs, which will be examined later. In any case, the similarity between the TA kinetics and the PPPC kinetics indicate that CTSs generation is governed by the same mechanism in films and devices.

Figure 5 (a) Comparing the early time pump-push-photocurrent kinetics (red) and the deconvoluted charge generation kinetics (blue) extracted from the TA data for the PffBT4T-2OD:EH-IDTBR device. Samples were excited at 650 nm and measured at room temperature. (b) T-dependent pump-push-photocurrent kinetics for PffBT4T-2OD:EH-IDTBR between 168 K and 291 K. (c) Arrhenius plot of the ln value of the $\Delta J/J$ amplitude at 2 ps (extracted from Figure 5b) as a function of the reciprocal T represented by the black square symbols. Solid lines indicate the linear fitting based on the equation $ln(-\frac{\Delta J}{J}) = -\frac{E_a}{k_B T}$, where k_B is the Boltzmann constant. Linear fittings in the high temperature regime (orange solid line) and the low temperature regime (blue solid line) yield an activation energy of 100 and 14 meV respectively.

Figure 5b presents the PPPC kinetics at different temperatures for the PffBT4T-2OD:EH-IDTBR device. Both the amplitude ($\Delta J/J$) and kinetics depend on the T. To understand the T-effect, we examine kinetics in two separate time regimes: before 100 ps and after 500 ps. The signal before 100 ps is likely to be associated with freshly generated bound CTSs. As expected, the peak amplitude increases as the T decreases, reflecting an increase in the population of CTSs. At lower temperatures, fewer CTSs can overcome the electrostatic barrier and directly dissociate into free

ACCEPTED MANUSCRIPT

AIP Publishing

This manuscript was accepted by J. Chem. Phys. Click here to see the version of record.

carriers. Therefore, the push pulse has a greater impact at low temperatures since there are more bound CTSs that can be dissociated, hence increasing the amplitude of PPPC signal. For a more quantitative analysis of the *T*-dependence, we apply an Arrhenius plot approach as shown in Figure 5c. Based on our previous work,[44] we extracted the amplitude at early time from Figure 5b and plotted it against the reciprocal *T*. The dependence can be described by two activation energies. At temperatures above 200 K, the dominant process responsible for the charge trapping has an E_a of 100 meV, which is attributed to the binding energy of CTSs. Below 200 K, the behaviour changes, and carrier extraction is limited by a different process with an E_a of 14 meV limits carrier extraction, which is discussed further below.

After a few hundred ps, the signal flattens out (and even exhibits minor growth), which was previously attributed to charge trapping.[45] Indeed, the *T*-dependence of the PPPC signal measured at 600 ps reveals a lower activation energy of 14 meV which is typical for the trapping of free carriers during charge transport. Though the push pulse has minimal effect on mobile carriers near the band edge,[44] it is able to elevate free carriers from low energy states to mobilize them again and thus generate additional photocurrent.[45] We therefore attribute this late-time signal to the de-trapping of separated charges. We note that this E_a is the same as the 14 meV observed for early-time data at temperatures below 200 K. We therefore conclude that at low temperatures carrier trapping can be as important for charge separation as the CTS binding energy.

Evaluation of the activation energy has been a long-standing question in application to polymer-polymer and polymer-fullerene OPVs and various values have been reported based on different techniques. For example, Gelinas *et al.* have reported a binding energy of 250 meV for CTSs in PFB:F8BT system using PL and TA over the ns time window.[46] Gao *et al.* have also interpreted the activation energy for charge separation to be between 9-25 meV depending on the morphology of the P3HT:$PC_{60}BM$ with EQE.[17] More recently, Neher and coworkers have reported the activation energy for charge formation from thermalized CTSs to be around 25 meV using time-delayed collection field (TDCF).[20] The activation energy values vary depending on the technique and the timescale selected. In our work, we probe the CTS behaviour at relatively early-times, exclusively involving charge generation from bound states. This differs from values extracted from other techniques that usually address a steady-state material/device performance that is controlled by a combination of electronic processes. We realize the reported 100 meV dissociation energy of

ACCEPTED MANUSCRIPT

AIP Publishing

This manuscript was accepted by J. Chem. Phys. Click here to see the version of record.

CTSs is similar to other fullerene systems, which indicates the smaller driving force has little effect of generation of CTSs. In some fullerene-based blends, charge generation also show independence on the energetic offsets.[47] Herein, we present the first report of binding energy for CTSs in NFA-based OPVs with a small driving force for charge separation.

Bringing together the PL, TA and PPPC results, we propose Figure 6 as a model for charge generation in PffBT4T-2OD:EH-IDTBR. Upon illumination, (a) excitons are formed in both PffBT4T-2OD and EH-IDTBR. Due to the similar singlet exciton energies, energy transfer occurs between PffBT4T-2OD and EH-IDTBR. (b) Excitons dissociate at the D/A interface within 15 ps to form bound CTSs. (c) A significant fraction of the initially formed CTSs undergo rapid internal conversion to lower localized states. (d) Another portion of the initially formed CTSs directly separate into free carriers. (e) When the push pulse arrives, localized CTSs can be excited to higher energy states to dissociate into free carriers. (f) The subsequent dissociation of CTSs into free carriers happens with different efficiencies depending on *T*. The activation barrier has been found to be 100 meV from *T*-dependent PPPC measurements. (g) A portion of CTSs remain bound and recombine over 1.2 ns. (h) Free carriers transport including trapping, de-trapping and hoping between different states. The trap depth has been estimated to be 14 meV. (i) Free carriers can then undergo bimolecular recombination or extraction to the electrodes.

Figure 6 Proposed model for charge carrier dynamics in OPV blends with a small driving force for charge separation and overlapping absorption profiles. In PffBT4T-2OD:EH-IDTBR blend: (a) Both D and A excitons exist upon photoexcitation and undergo energy transfer with each other. (b) Dissociation of excitons at the interface to form CTSs. CTSs can either (c) relax into localized states or (d) separate into free carriers. (e) and (f) The push pulse (0.6 eV) excites localized CTSs to higher energetic states and dissociate into free carriers. this dissociation has an activation energy of 100 meV. (g) Geminate recombination of CTSs govern the main recombination pathway in this blend. (h) Carriers hop and de-trap with a trap depth of 14 meV. (i) Carriers will go through bimolecular recombination if not being extracted out of the electrodes.

V. Conclusion

In conclusion, we employed two spectroscopy tools, TA and PPPC, to elucidate the charge carrier dynamics in a NFA OPV blend PffBT4T-2OD:EH-IDTBR. The results indicate rapid energy transfer between PffBT4T-2OD excitons and EH-IDTBR excitons following photoexcitation. The dissociation of excitons at the interface generates CTSs slowly with a time constant of 15 ps. We

ACCEPTED MANUSCRIPT

AIP Publishing

This manuscript was accepted by J. Chem. Phys. Click here to see the version of record.

have also clarified that the same mechanism governs the charge generation in both blend films and devices. The main loss mechanism in PffBT4T-2OD:EH-IDTBR blend is geminate recombination of charges occurring on the timescale of 1 ns. *T*-dependent PPPC suggests a relatively low CT exciton binding energy of 100 ± 6 meV for the dissociation of CTSs. We also observed a long-time rise in PPPC response which we attribute to the charge trapping with a trap activation energy of 14 ± 7 meV. Together with the reasonably high PL quenching yield, our results suggest that the main limiting factor in PffBT4T-2OD:EH-IDTBR performance is not the exciton dissociation but the ability of charges to escape from the D/A interface.

Experimental section:

Materials: PffBT4T-2OD and $PC_{71}BM$ were purchased from Ossila and 1-Material respectively. EH-IDTBR was prepared according to previously reported procedure.[10]

Film preparation: PffBT4T-2OD and $PC_{71}BM$ (D:A weight ratio 1:1.4) blend solution (polymer D concentration: 10 mg mL^{-1}) was prepared in CB and DCB (1:1 volume ratio) with 3 vol% 1,8-diiodooctane. PffBT4T-2OD and EH-IDTBR (D:A weight ratio 1:1.2) blend solution (polymer D concentration: 10 mg mL^{-1}) was prepared in DCB. Active layer solutions were stirred on a hot plate at 110 °C for 1 hour and then at 60 °C overnight. Prior to spin coating on to the preheated glass substrates (80 °C) at 1500 rpm in a nitrogen glovebox, the solutions were reheated to 110 °C.

Device fabrication: Devices were fabricated in an inverted architecture (ITO/ZnO/ PffBT4T-2OD:acceptor/MoO_3/Ag). ITO substrates were cleaned with soap, water, acetone and isopropanol. They were then treated with oxygen plasma prior to spin coating of zinc acetate dihydrate precursor solution (60.4 μL 1-ethanolamine in 2 mL 2-methoxyethanol). ZnO layers were annealed at 150 °C for 10 mins. Blend solutions were prepared in the same way as previously described for film preparation. They were spun onto the ITO substrates at 1500 rpm in a nitrogen glovebox. MoO_3 (10 nm) and Ag (100 nm) layers were deposited by vacuum evaporation through a mask with an active area of 0.045 cm^2 in each device. Current-voltage characteristics were measured with a Keithley 2400 source meter under AM 1.5 illumination from a Xenon lamp (Oriel Instruments).

UV-Vis absorbance spectroscopy: A PerkinElmer Lambda 25 spectrometer was used to carry out UV-Vis absorbance for thin film samples.

ACCEPTED MANUSCRIPT

AIP Publishing

This manuscript was accepted by J. Chem. Phys. Click here to see the version of record.

Steady state photoluminescence spectroscopy: Steady-state PL spectra were measured on a Fluorolog-3 spectrofluorometer (FL 3-22, Horiba Jobin Yvon). All the samples were excited at 600 nm with a slit width of 5 nm. The emitted photons were collected in the front-face geometry with a slit width of 5 nm.

Time correlated single photon counting: The DeltaFlex TCSPC system (Horiba Scientific) was used to measure the PL kinetics of thin film samples. Samples were excited by a NanoLED at 635 nm. Photons were detected with a PPD detector up to 950 nm. The instrument temporal resolution is 100 fs.

Transient absorption spectroscopy: A broadband pump-probe fs TA spectrometer Helios (Spectra Physics, Newport Corp.) was used to measure the TA spectra and kinetics for thin film samples. Ultrafast laser pulses (800 nm, 100 fs pulse duration) were generated by a 1 kHz Ti:sapphire regenerative amplifier (Solstice, Spectra Physics). One portion of the 800-nm pulses was directed to an optical parametric amplifier (TOPAS) to generate the visible pump pulses at 700 nm. The rest of the 800 nm pulses routes onto a mechanical delay stage (6 ns time window) and is directed through a sapphire crystal to generate white light probe ranging from 800 to 1600 nm in the near-infrared region. The pump and probe beams were focused onto the same spot on the samples. During the measurements, all the samples were kept in a quartz cuvette under continuous N_2 flow.

Pump-push-photocurrent spectroscopy: fs-pulses (800 nm, 35 fs) were generated by a 4 kHz Ti:sapphire regenerative amplifier (Astrella, Coherent). These pulses are routed onto two optical parametric amplifiers (TOPAS Prime, Coherent). The 1200 nm output from one TOPAS passed through a frequency-doubling barium borate (BBO) crystal to generate the pump at 600 nm. The pump pulse was then directed onto a mechanical delay stage to vary the time delay between the pump and the push beams. The 2000 nm output from the other TOPAS serves as the push. The push was mechanically modulated at 1.1 kHz. Both the pump and push pulses were aligned onto a single spot on the device pixel. During the measurements, the devices were connected to a lock-in amplifier (SR830, Stanford Research Systems) and were measured under short-circuit conditions. The reference current J is measured at the pump frequency of 4 kHz and the push induced current ΔJ was measured at the push frequency of 1.1 kHz.

ACCEPTED MANUSCRIPT

AIP Publishing

This manuscript was accepted by J. Chem. Phys. Click here to see the version of record.

Global analysis: Global analysis was carried out using a previously written programme based on a genetic algorithm.[46] We first extract the spectra of singlet excitons of D and A from TA measurement of the neat materials. As a time-efficient approach, we use those as initial guesses and add on randomness into each species. Throughout the fitting, the algorithm examines the fitness of each and reaches the most fitted result.

Supplementary Materials

Time-resolved PL of neat materials and blend materials; time-resolved emission spectra of neat materials and the blend materials; normalised TA spectra for neat materials and the blend materials; TEM of blend materials.

Acknowledgements

The authors would like to thank Tom Hopper, Dr. Robert Godin and Dr. Wenxing Yang for discussions. The authors would also like to thank Tom Hopper for proofreading the manuscript and Ahmad Alraddadi for TEM. The authors acknowledge Optoelectronics Group in the University of Cambridge for sharing the software for global analysis. A.A.B. is a Royal Society University Research Fellow. J.Z. thanks the China Scholarship Council for a PhD scholarship (No. 201503170255).

Conflict of interests

The authors declare no competing financial interest.

References

1 G. Yu, J. Gao, J. C. Hummelen, F. Wudl and A. J. Heeger, *Science (80-.).*, 1995, **270**, 1789–1791.

2 A. Wadsworth, M. Moser, A. Marks, M. S. Little, N. Gasparini, C. J. Brabec, D. Baran and I. McCulloch, *Chem. Soc. Rev.*, 2018.

3 Y. Lin, J. Wang, Z.-G. Zhang, H. Bai, Y. Li, D. Zhu and X. Zhan, *Adv. Mater.*, 2015, **27**, 1170–1174.

4 C. Yan, S. Barlow, Z. Wang, H. Yan, A. K. Y. Jen, S. R. Marder and X. Zhan, *Nat. Rev. Mater.*, 2018, **3**, 1–19.

5 J. Hou, O. Inganäs, R. H. Friend and F. Gao, *Nat. Mater.*, 2018, **17**, 119–128.

6 W. Zhao, D. Qian, S. Zhang, S. Li, O. Ingan??s, F. Gao and J. Hou, *Adv. Mater.*, 2016, **28**, 4734–4739.

ACCEPTED MANUSCRIPT

AIP Publishing

This manuscript was accepted by J. Chem. Phys. Click here to see the version of record.

7 D. Sun, D. Meng, Y. Cai, B. Fan, Y. Li, W. Jiang, L. Huo, Y. Sun and Z. Wang, *J. Am. Chem. Soc.*, 2015, **137**, 11156–11162.

8 D. Baran, N. Gasparini, A. Wadsworth, C. H. Tan, N. Wehbe, X. Song, Z. Hamid, W. Zhang, M. Neophytou, T. Kirchartz, C. J. Brabec, J. R. Durrant and I. McCulloch, *Nat. Commun.*, 2018, **9**, 1–9.

9 H. Cha, J. Wu, A. Wadsworth, J. Nagitta, S. Limbu, S. Pont, Z. Li, J. Searle, M. F. Wyatt, D. Baran, J.-S. Kim, I. McCulloch and J. R. Durrant, *Adv. Mater.*, 2017, **29**, 1701156.

10 S. Holliday, R. S. Ashraf, A. Wadsworth, D. Baran, S. A. Yousaf, C. B. Nielsen, C.-H. Tan, S. D. Dimitrov, Z. Shang, N. Gasparini, M. Alamoudi, F. Laquai, C. J. Brabec, A. Salleo, J. R. Durrant and I. McCulloch, *Nat. Commun.*, 2016, **7**, 11585.

11 L. Meng, Y. Zhang, X. Wan, C. Li, X. Zhang, Y. Wang, X. Ke, Z. Xiao, L. Ding, R. Xia, H.-L. Yip, Y. Cao and Y. Chen, *Science (80-.).*, 2018, **361**, 1094–1098.

12 W. Zhao, D. Qian, S. Zhang, S. Li, O. Inganäs, F. Gao and J. Hou, *Adv. Mater.*, 2016, 4734–4739.

13 Z. Fei, F. D. Eisner, X. Jiao, M. Azzouzi, J. A. Röhr, Y. Han, M. Shahid, A. S. R. Chesman, C. D. Easton, C. R. McNeill, T. D. Anthopoulos, J. Nelson and M. Heeney, *Adv. Mater.*, 2018, **30**, 1–7.

14 F. Zhao, S. Dai, Y. Wu, Q. Zhang, J. Wang, L. Jiang, Q. Ling, Z. Wei, W. Ma, W. You, C. Wang and X. Zhan, *Adv. Mater.*, 2017, **29**, 1–7.

15 N. Gasparini, M. Salvador, S. Strohm, T. Heumueller, I. Levchuk, A. Wadsworth, J. H. Bannock, J. C. de Mello, H. J. Egelhaaf, D. Baran, I. McCulloch and C. J. Brabec, *Adv. Energy Mater.*, 2017, **7**, 1–7.

16 S. Zhang, Y. Qin, J. Zhu and J. Hou, *Adv. Mater.*, 2018, **30**, 1–7.

17 F. Gao, W. Tress, J. Wang and O. Inganäs, *Phys. Rev. Lett.*, 2015, **114**, 1–5.

18 Y. Puttisong, Y. Xia, X. Chen, F. Gao, I. A. Buyanova, O. Inganäs and W. M. Chen, *J. Phys. Chem. C*, 2018, **122**, 12643–12646.

19 H. Bässler and A. Kohler, *Phys. Chem. Chem. Phys.*, 2015, **17**, 28451–28462.

20 J. Kurpiers, T. Ferron, S. Roland, M. Jakoby, T. Thiede, F. Jaiser, S. Albrecht, S. Janietz, B. A. Collins, I. A. Howard and D. Neher, *Nat. Commun.*, 2018, **9**, 1–11.

21 J. Benduhn, K. Tvingstedt, F. Piersimoni, S. Ullbrich, Y. Fan, M. Tropiano, K. A. McGarry, O. Zeika, M. K. Riede, C. J. Douglas, S. Barlow, S. R. Marder, D. Neher, D. Spoltore and K. Vandewal, *Nat. Energy*, 2017, **2**.

22 D. Qian, Z. Zheng, H. Yao, W. Tress, T. R. Hopper, S. Chen, S. Li, J. Liu, S. Chen, J. Zhang, X. K. Liu, B. Gao, L. Ouyang, Y. Jin, G. Pozina, I. A. Buyanova, W. M. Chen, O. Inganäs, V. Coropceanu, J. L. Bredas, H. Yan, J. Hou, F. Zhang, A. A. Bakulin and F. Gao, *Nat. Mater.*, 2018, **17**, 703–709.

23 T. M. Burke, S. Sweetnam, K. Vandewal and M. D. McGehee, *Adv. Energy Mater.*, 2015,

ACCEPTED MANUSCRIPT

AIP Publishing

This manuscript was accepted by J. Chem. Phys. Click here to see the version of record.

5, 1–12.

24 K. Vandewal, K. Tvingstedt, A. Gadisa, O. Inganäs and J. V Manca, *Nat. Mater.*, 2009, **8**, 904–909.

25 S. Chen, Y. Wang, L. Zhang, J. Zhao, Y. Chen, D. Zhu, H. Yao, G. Zhang, W. Ma, R. H. Friend, P. C. Y. Chow, F. Gao and H. Yan, *Adv. Mater.*, 2018, **1804215**, 1804215.

26 S. M. Menke, N. A. Ran, G. C. Bazan and R. H. Friend, *Joule*, 2017, 1–11.

27 Y. Liu, J. Zhao, Z. Li, C. Mu, W. Ma, H. Hu, K. Jiang, H. Lin, H. Ade and H. Yan, *Nat. Commun.*, 2014, **5**, 1–8.

28 H. Cha, C.-H. Tan, J. Wu, Y. Dong, W. Zhang, H. Chen, S. Rajaram, K. S. Narayan, I. McCulloch and J. R. Durrant, *Adv. Energy Mater.*, 2018, **1801537**, 1–9.

29 H. Cha, J. Wu, A. Wadsworth, J. Nagitta, S. Limbu, S. Pont, Z. Li, J. Searle, M. F. Wyatt, D. Baran, J. S. Kim, I. McCulloch and J. R. Durrant, *Adv. Mater.*, 2017, **29**.

30 L. Krückemeier, P. Kaienburg, J. Flohre, K. Bittkau, I. Zonno, B. Krogmeier and T. Kirchartz, *Commun. Phys.*, 2018, **1**, 27.

31 Y. Lin, F. Zhao, S. K. K. Prasad, J.-D. Chen, W. Cai, Q. Zhang, K. Chen, Y. Wu, W. Ma, F. Gao, J.-X. Tang, C. Wang, W. You, J. M. Hodgkiss and X. Zhan, *Adv. Mater.*, 2018, **30**, 1706363.

32 M. A. Alamoudi, J. I. Khan, Y. Firdaus, K. Wang, D. Andrienko, P. M. Beaujuge and F. Laquai, *ACS Energy Lett.*, 2018, **3**, 802–811.

33 A. Weu, T. R. Hopper, V. Lami, J. A. Kreß, A. A. Bakulin and Y. Vaynzof, *Chem. Mater.*, 2018, **30**, 2660–2667.

34 I. A. Howard, R. Mauer, M. Meister and F. Lacquai, *J. Am. Chem. Soc.*, 2010, **132**, 14866–14876.

35 A. J. Ward, A. Ruseckas, M. M. Kareem, B. Ebenhoch, L. A. Serrano, M. Al-Eid, B. Fitzpatrick, V. M. Rotello, G. Cooke and I. D. W. Samuel, *Adv. Mater.*, 2015, **27**, 2496–2500.

36 J. L. Brédas, E. H. Sargent and G. D. Scholes, *Nat. Mater.*, 2016, **16**, 35–44.

37 F. Etzold, I. A. Howard, R. Mauer, M. Meister, T. D. Kim, K. S. Lee, N. S. Baek and F. Laquai, *J. Am. Chem. Soc.*, 2011, **133**, 9469–9479.

38 T. M. Clarke and J. R. Durrant, *Chem. Rev.*, 2010, **110**, 6736–6767.

39 S. M. Menke, A. Cheminal, P. Conaghan, N. A. Ran, N. C. Greehnam, G. C. Bazan, T. Q. Nguyen, A. Rao and R. H. Friend, *Nat. Commun.*, 2018, **9**, 1–7.

40 T. M. Clarke, A. M. Ballantyne, S. Tierney, M. Heeney, W. Duffy, I. McCulloch, J. Nelson and J. R. Durrant, *J. Phys. Chem. C*, 2010, **114**, 8068–8075.

41 A. A. Bakulin, A. Rao, V. G. Pavelyev, P. H. M. van Loosdrecht, M. S. Pshenichnikov, D. Niedzialek, J. Cornil, D. Beljonne and R. H. Friend, *Science (80-.).*, 2012, **335**, 1340–

ACCEPTED MANUSCRIPT

AIP Publishing

This manuscript was accepted by J. Chem. Phys. Click here to see the version of record.

1344.

42 Y. Liu, L. Zuo, X. Shi, A. K.-Y. Jen and D. S. Ginger, *ACS Energy Lett.*, 2018, 2396–2403.

43 J. Zhang, Q. Gu, T. T. Do, K. Rundel, P. Sonar, R. H. Friend, C. R. McNeill and A. A. Bakulin, *J. Phys. Chem. A*, 2018, **122**, 1253–1260.

44 J. Zhang, A. C. Jakowetz, G. Li, D. Di, S. M. Menke, A. Rao, R. H. Friend and A. A. Bakulin, *J. Mater. Chem. A*, 2017, **5**, 11949–11959.

45 A. A. Bakulin, S. Neutzner, H. J. Bakker, L. Ottaviani, D. Barakel and Z. Chen, *ACS Nano*, 2013, **7**, 8771–8779.

46 S. Gélinas, O. Paré-Labrosse, C. N. Brosseau, S. Albert-Seifried, C. R. McNeill, K. R. Kirov, I. A. Howard, R. Leonelli, R. H. Friend and C. Silva, *J. Phys. Chem. C*, 2011, **115**, 7114–7119.

47 A. C. Jakowetz, M. L. Böhm, J. Zhang, A. Sadhanala, S. Huettner, A. A. Bakulin, A. Rao and R. H. Friend, *J. Am. Chem. Soc.*, 2016, **138**, 11672–11679.

ACCEPTED MANUSCRIPT

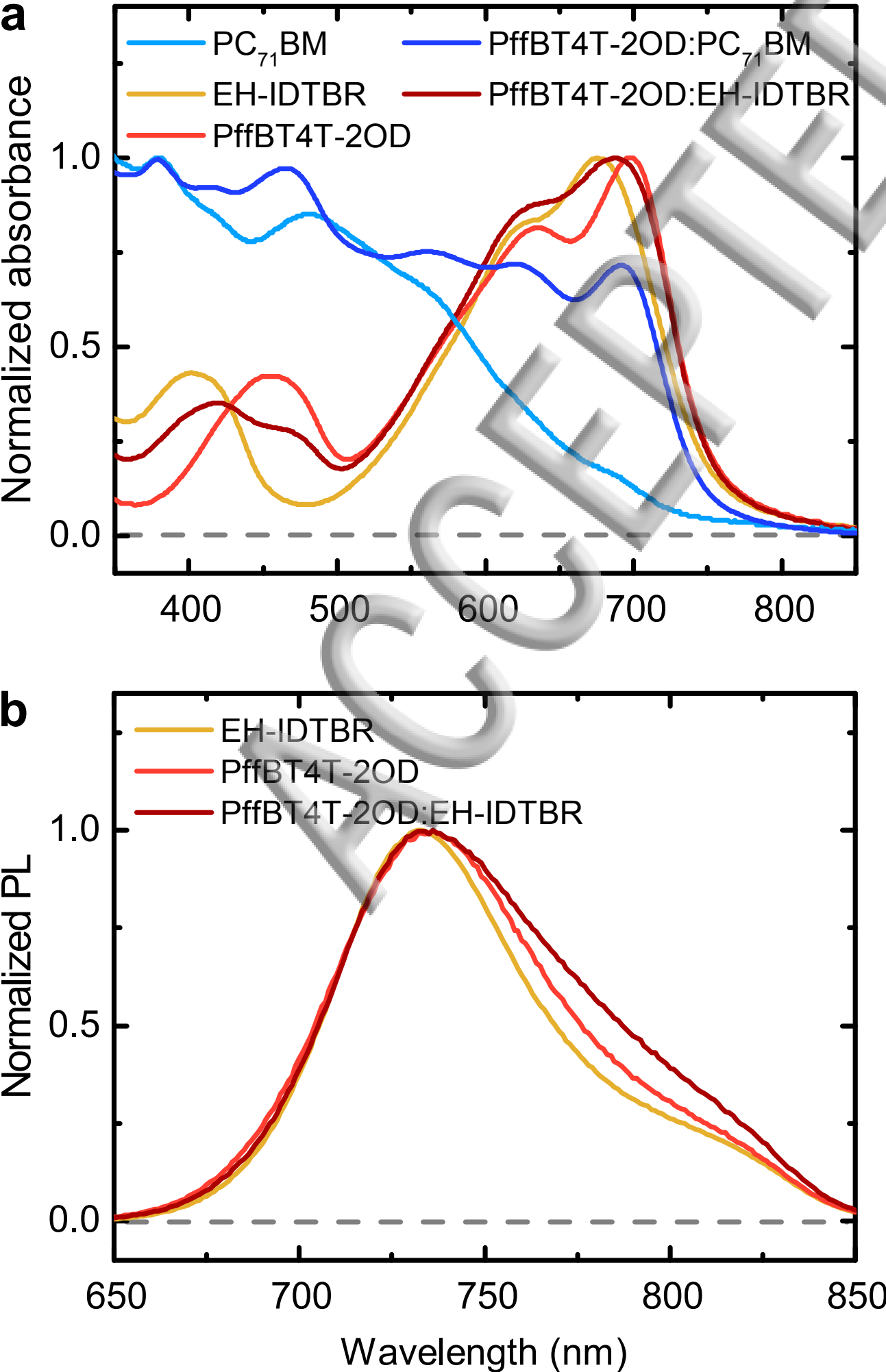
a
PC71BM
PffBT4T-2OD:PC71BM
EH-IDTBR
PffBT4T-2OD:EH-IDTBR
PffBT4T-2OD
Normalized absorbance
1.0
0.5
0.0
400
500
600
700
800
b
EH-IDTBR
PffBT4T-2OD
PffBT4T-2OD:EH-IDTBR
Normalized PL
1.0
0.5
0.0
650
700
750
800
850
Wavelength (nm)
ACCEPTED

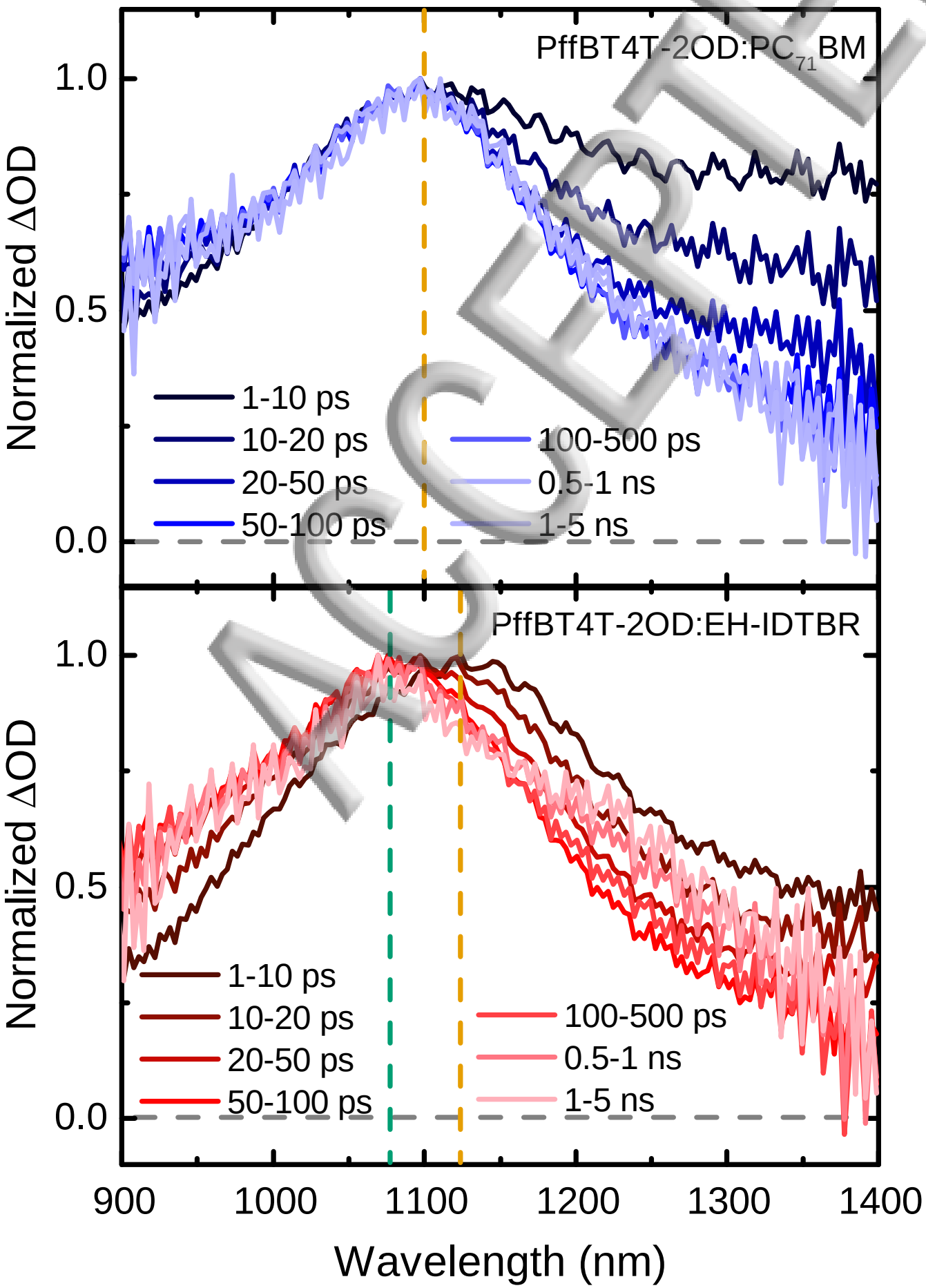
PffBT4T-2OD:PC71BM
1-10 ps
10-20 ps
20-50 ps
50-100 ps
100-500 ps
0.5-1 ns
1-5 ns
PffBT4T-2OD:EH-IDTBR
1-10 ps
10-20 ps
20-50 ps
50-100 ps
100-500 ps
0.5-1 ns
1-5 ns
Normalized ΔOD
1.0
0.5
0.0
900
1000
1100
1200
1300
1400
Wavelength (nm)

ACCEPTED

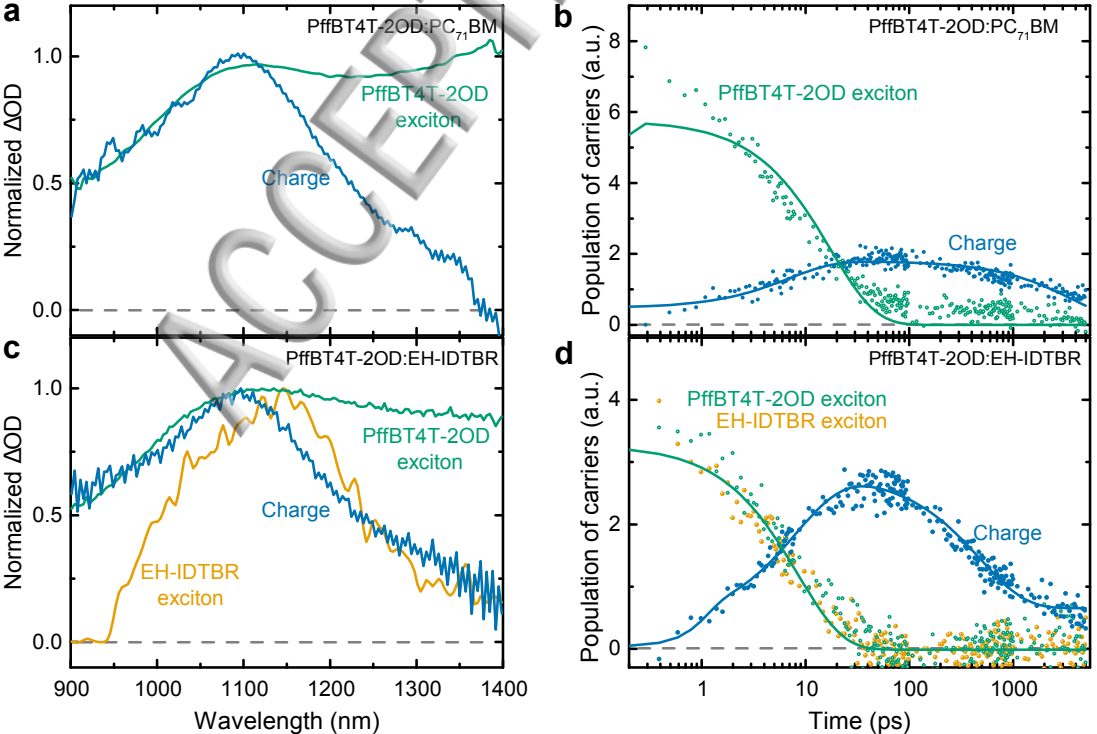
a
PffBT4T-2OD:PC71BM
PffBT4T-2OD exciton
Charge
Normalized ΔOD
b
PffBT4T-2OD:PC71BM
PffBT4T-2OD exciton
Charge
Population of carriers (a.u.)
c
PffBT4T-2OD:EH-IDTBR
PffBT4T-2OD exciton
Charge
EH-IDTBR exciton
Normalized ΔOD
d
PffBT4T-2OD:EH-IDTBR
PffBT4T-2OD exciton
EH-IDTBR exciton
Charge
Population of carriers (a.u.)
Wavelength (nm)
Time (ps)

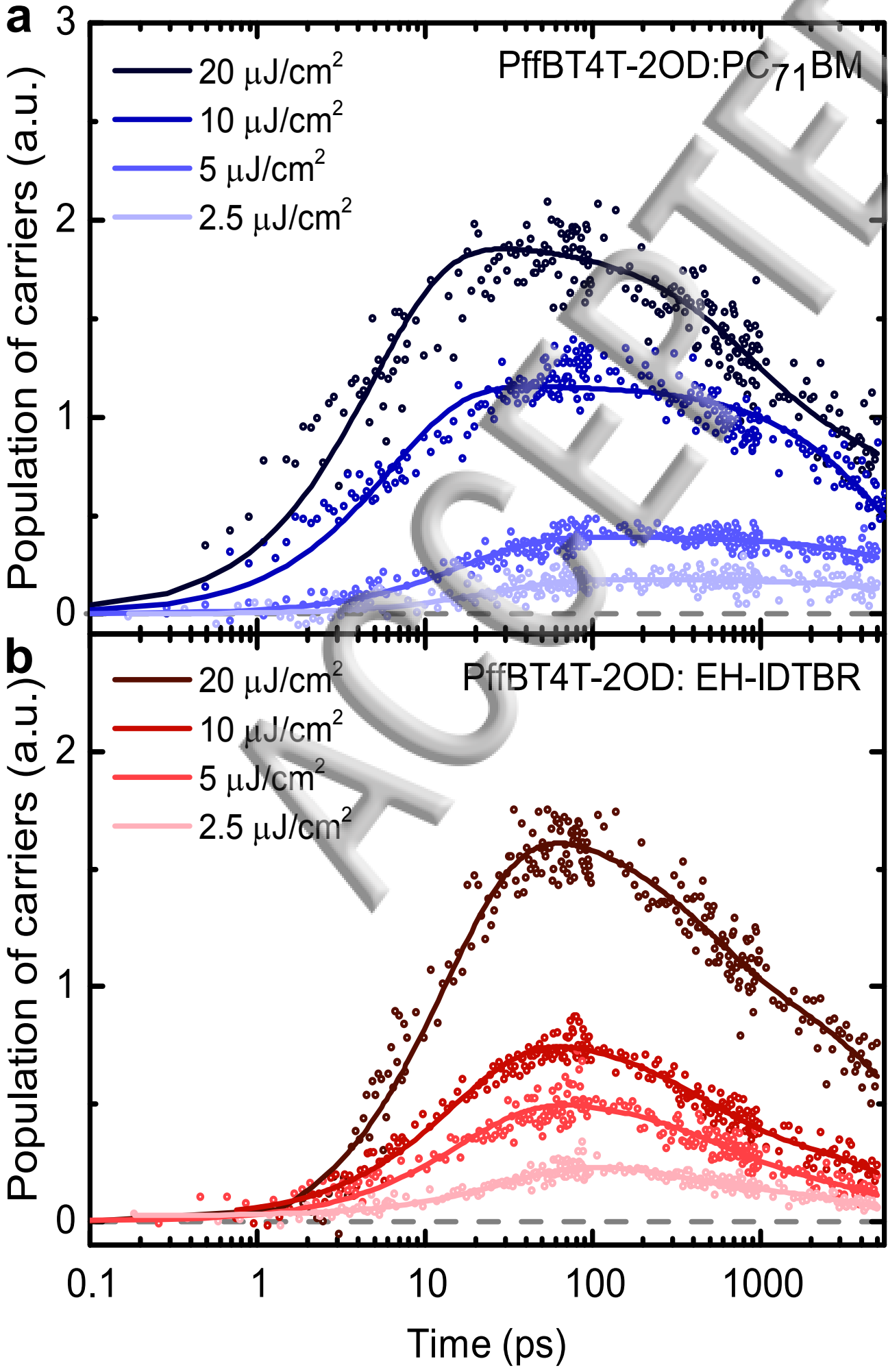
a
PffBT4T-2OD:PC71BM
20 μJ/cm2
10 μJ/cm2
5 μJ/cm2
2.5 μJ/cm2
Population of carriers (a.u.)
b
PffBT4T-2OD: EH-IDTBR
20 μJ/cm2
10 μJ/cm2
5 μJ/cm2
2.5 μJ/cm2
Population of carriers (a.u.)
0.1
1
10
100
1000
Time (ps)
ACCEPTED

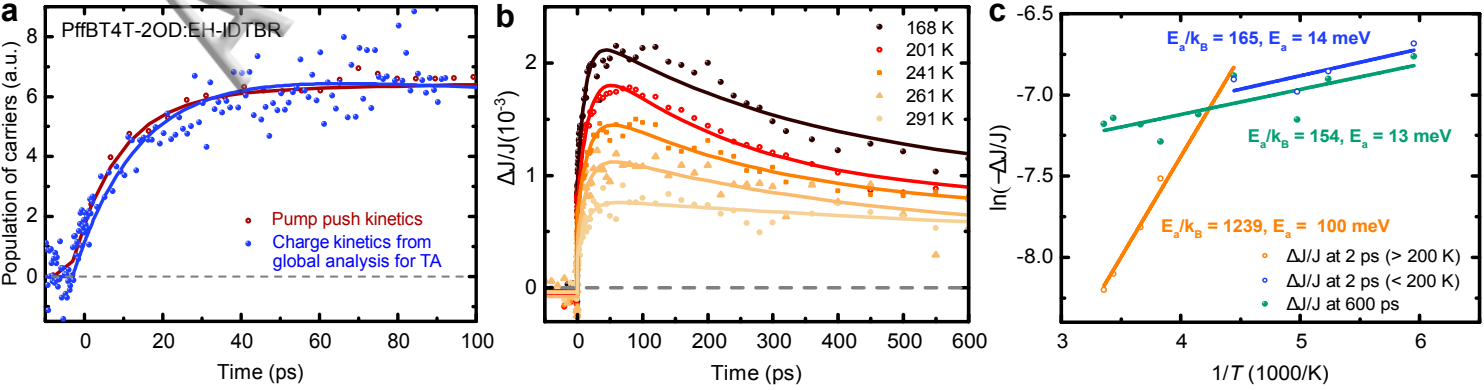
a
PffBT4T-2OD:EH-IDTBR
Population of carriers (a.u.)
Time (ps)
Pump push kinetics
Charge kinetics from global analysis for TA
b
ΔJ/J(10^-3)
Time (ps)
168 K
201 K
241 K
261 K
291 K
c
ln(−ΔJ/J)
1/T (1000/K)
E_a/k_B = 165, E_a = 14 meV
E_a/k_B = 154, E_a = 13 meV
E_a/k_B = 1239, E_a = 100 meV
ΔJ/J at 2 ps (> 200 K)
ΔJ/J at 2 ps (< 200 K)
ΔJ/J at 600 ps

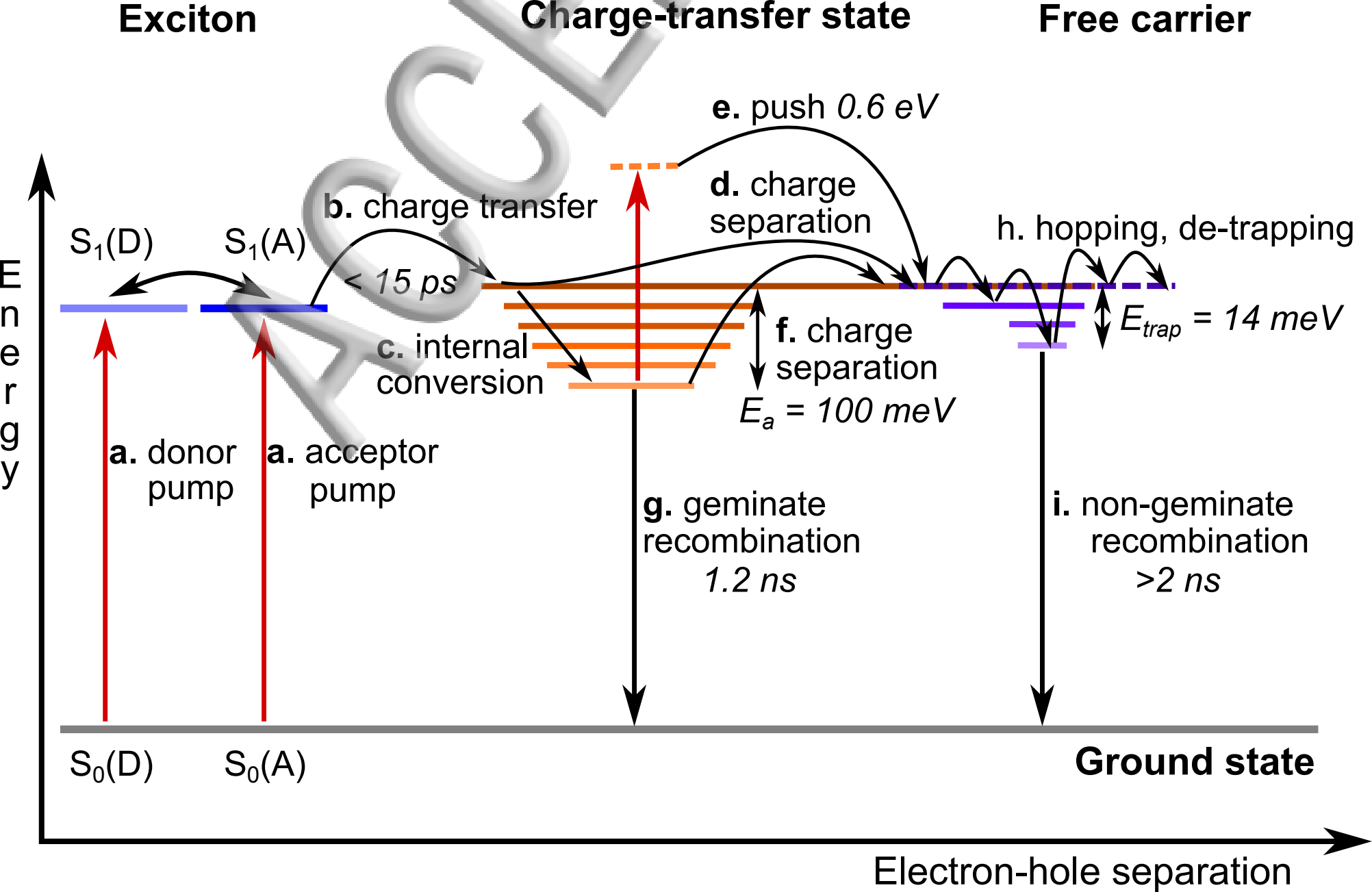
Exciton
Charge-transfer state
Free carrier
e. push 0.6 eV
d. charge separation
b. charge transfer
h. hopping, de-trapping
S1(D)
S1(A)
< 15 ps
Energy
c. internal conversion
f. charge separation
Ea = 100 meV
Etrap = 14 meV
a. donor pump
a. acceptor pump
g. geminate recombination 1.2 ns
i. non-geminate recombination >2 ns
S0(D)
S0(A)
Ground state
Electron-hole separation